SUPPLEMENTARY FIGURE LEGENDS

Supplementary Figure 1. ATF4 is a strong candidate to be responsible for the transcription dysregulation in mutant *DISC1* neurons. (**a**) Venn diagram showing 8 proteins in DISC1 interactome are transcription factors. (**b**) Venn diagram showing 221 genes dysregulated in mutant *DISC1* neurons (D2) are ATF4 ChIP targets according to the GTRD database. (**c**) Nuclear ATF4, including nuclear soluble and chromatin bound protein, is more enriched in D2 neurons than that in C3 neurons. Values represent mean ± s.e.m. (n = 3; *p < 0.05; ***p < 0.001; t-test)

Supplementary Figure 2. Differentiation of iPSCs into glutamatergic cortical neurons. (**a-c**) Sample confocal images of cultures upon differentiation of iPSCs following our previous published protocol, showing immunostaining for GABAergic neuron marker GABA, glutamatergic neuron marker CAMKII, neuronal marker DCX (**a**), cortical layer markers CTIP2 (**b**) and Tbr2 (**c**). Scale bar: 50 μm. (**d**) Quantification of percentages of cells exhibiting specific neuronal markers upon differentiation of C3 and D2 iPSC lines. Values represent mean ± s.e.m. (n = 3).

Supplementary Figure 3. Features of gene dysregulation shared between mutant *DISC1* neurons (D2) and control neurons with ATF4 overexpression (C3+ATF4 OE). (**a**) Heatmap of sample distance and similarity matrix based on RNA sequencing results of C3 (n = 3) and C3+ATF4 OE neurons (n = 3). (**b**) Heatmap of expression levels of overlapped 302 up- and 381 down-regulated genes in D2 and C3+ATF4 OE neurons. (**c**) Bubble plot of top 10 categories in GO analysis of 381 overlapped down-regulated genes in D2 and C3+ATF4 OE neurons. (**d**) Visualization of the top 10 pathways identified by KEGG analysis of total up-regulated genes in D2 (773 genes) and C3+ATF4 OE neurons (1861 genes). (**e**) Visualization of top 10 pathways in KEGG analysis of total down-regulated genes in D2 (1158 genes) and C3+ATF4 OE neurons (2030 genes).

Supplementary Figure 4. Promoter activity analysis using a dual-reporter luciferase system in the SH-SY5Y cell line. Luciferase assay shows increased *SYNPR* and *GRIN* transcriptional

activity with increasing ATF4 levels. Values represent mean ± s.e.m. (n = 3; *p < 0.05; **p < 0.01; ***p < 0.001; t-test)

Supplementary Figure 5. Generation of D2:ATF4$^{+/-}$ iPSCs by CRISPR/Cas9 system. (**a**) Schematic depiction of the dual-gRNA targeting strategy. (**b**) Sanger sequencing results confirming the correct sequence deletion. (**c**) Sample images of iPSCs immunostained with pluripotency marker SOX2 (green); OCT4 (red) and DAPI (blue). Scale bar: 20 μm. (**d**) Sample images of neural progenitors immunostained with NESTIN (green); PAX6 (red) and DAPI (blue). Scale bar: 20 μm. (**e**) Whole cell western blot shows ATF4 protein decrease after heterozygous gene knock-out in D2. (**f**) Western blot of subcellular protein shows nuclear soluble and chromatin bound ATF4 is significantly decreased in D2:ATF4$^{+/-}$ cells. Values represent mean ± s.e.m. (n = 6; *p < 0.05; ***p < 0.001; t-test)

Supplementary Figure 6. DISC1-CC and ATF4-LZ adopt a stable conformation with strong binding affinity. (**a**) Analytical gel filtration chromatography analysis coupled with static light scattering analysis of DISC1-CC (blue line), trx tagged-ATF4-LZ (red line) and the DISC1-CC/trx tagged-ATF4-LZ complex (dashed black line), which give rise to molecular weights listed in **Figure 3c**. (**b**) NMR 15N-HSQC spectra showing the DISC1-ATF4 fusion protein adopts a uniform conformation in solution. Assignments are shown with each residue name and number. Residues from DISC1 are labelled in red and residues from ATF4 are labelled in black. (**c**) Overlay of the 15N-HSQC spectra of the DISC1-ATF4 fusion protein (black) and DISC1 titrated with one molar ratio of an unlabeled ATF4 peptide (Red). The similar profile of peaks of DISC1-CC (particularly those in the structured regions) in the two spectra indicates that the fusion ATF4 to the C-terminal end of DISC1-CC does not alter the structure of the DISC1-CC/ATF4 complex.

Supplementary Figure 7. Details of the interactions mediating the DISC1/ATF4 complex formation. (**a**) Sequence alignment of DISC1 from different species. The secondary structural elements are indicated above the alignment. Residues corresponding to the heptad repeats (i.e. from a to e) of the coiled coils are indicated above the alignments. The conserved hydrophobic residues that are involved in the dimer interface are highlighted in yellow, positively charged

residues in blue and negatively charged residues in red. Mutations that disrupt or weaken the DISC1/ATF4 complex formation are highlighted with red stars. The sequence of DISC1 resulting from the frameshift mutation found in the American family patients is also shown (with 9 non-native residues shown in pink). (**b**) Sequence alignment of ATF4 from different species. The point mutation that disrupts the DISC1/ATF4 complex formation is highlighted with a red star. (**c**) Combined-surface and ribbon representation showing the conservation scale of DISC1 and ATF4 binding interface. In the surface diagram, the highly conserved amino acids are drawn in blue, the less conserved residues in orange. The residues involved in DISC1/ATF4 interaction interface are all evolutionarily conserved. (**d**) Combined surface and ribbon representation showing the interaction interface between DISC1 and ATF4. In the surface diagram, hydrophobic residues are colored in yellow, positively charged residues are colored in blue and negatively charged residues in red. (**e**) Open book view showing the binding interface of the DISC1/ATF4 complex. The main chains of DISC1 and ATF4 are drawn in a ribbon model and the side chains are drawn in a stick and sphere model. (**f**) Helical wheel representation showing the detailed interactions between the heptad repeats in the DISC1/ATF4 complex. Residues at the a and d positions forming the hydrophobic core of the coiled coil are highlighted in orange. Inter-helical interactions between the residues at the e and g (or even b in certain cases) positions are depicted by dashed lines. Residues forming electrostatic interactions are colored with blue for positively charged residues and red for negatively charged residues.

Supplementary Figure 8. Sequence integrity is required for the strong and specific binding between DISC1 and ATF4. (**a-c**) The ITC titration curves of the binding reactions that give rise to dissociation constants listed in **Figure 3f**. (**d**) DISC1 binds to other leucine zipper family transcription factors with very weak affinities. ITC titration curves showing the bindings of C/EBPα and C/EBPζ/CHOP with DISC1 are rather weak and with Kd of ~10 μM, which is ~2000-fold weaker than the ATF4 and DISC1 interaction.

Supplementary Movie 1: Neural network activity recorded using MEA under different culture conditions, included cortical neurons differentiated from C3, D2 iPSC lines and from C3 + ATF4E OE and D2:ATF4$^{+/-}$.

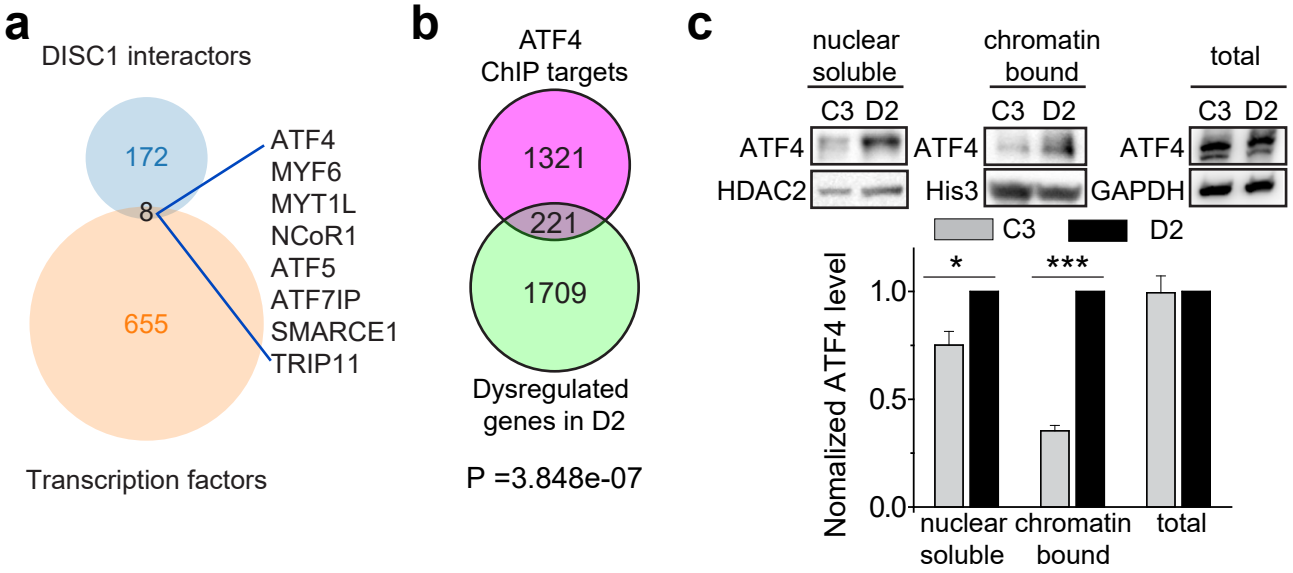

Supplementrary Figure 1 (Wang et al.)

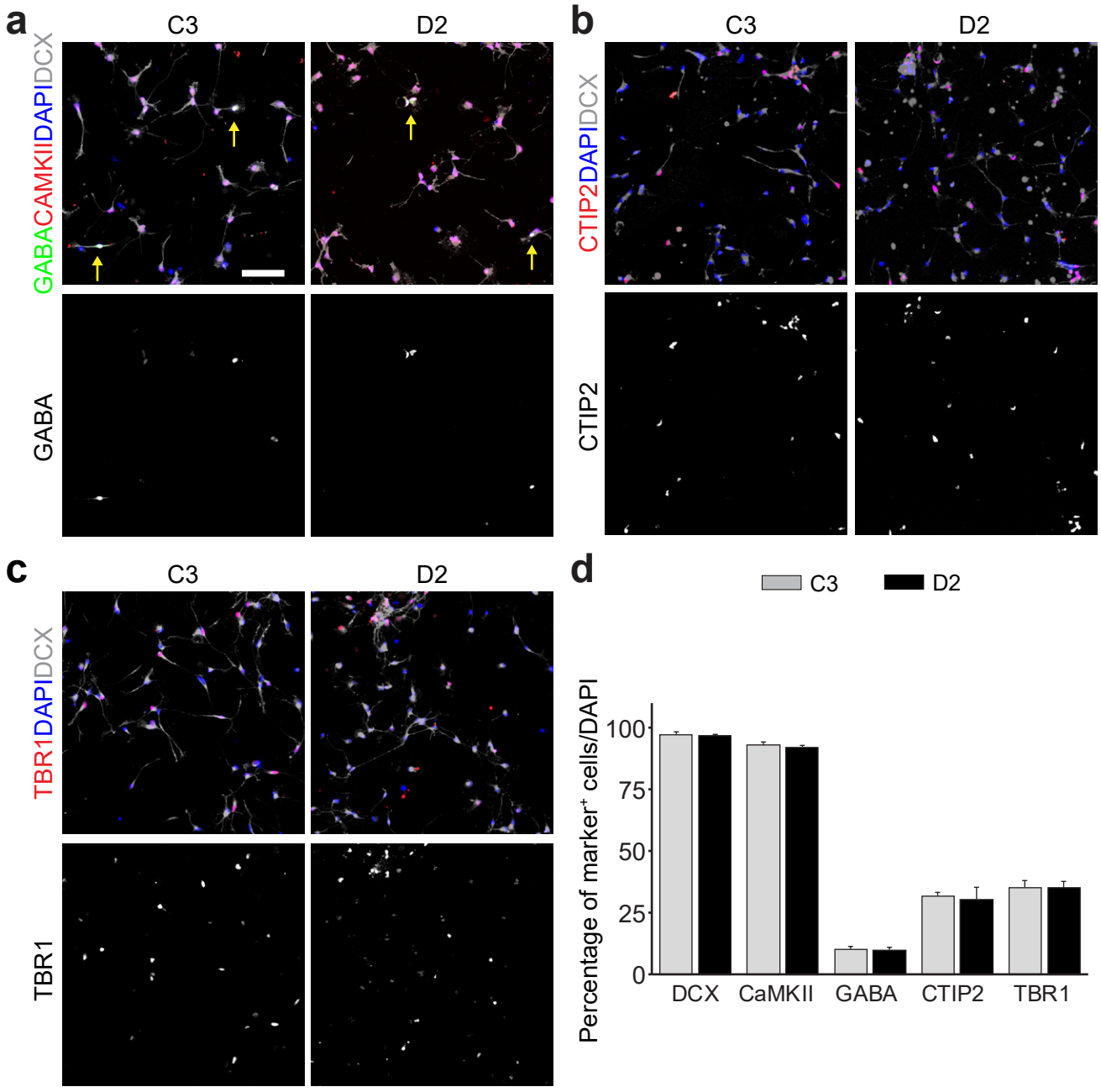

Supplementrary Figure 2 (Wang et al.)

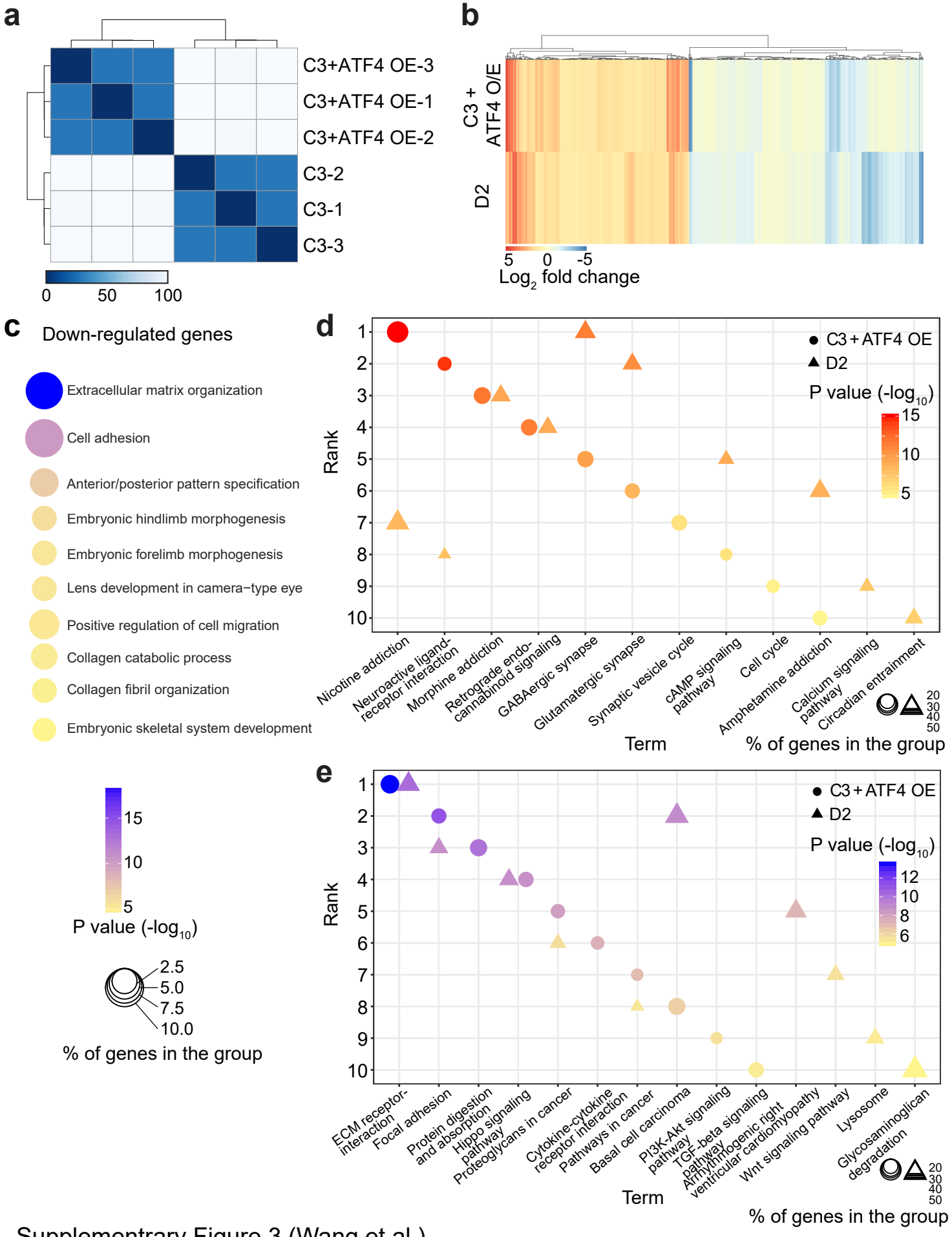

Supplementrary Figure 3 (Wang et al.)

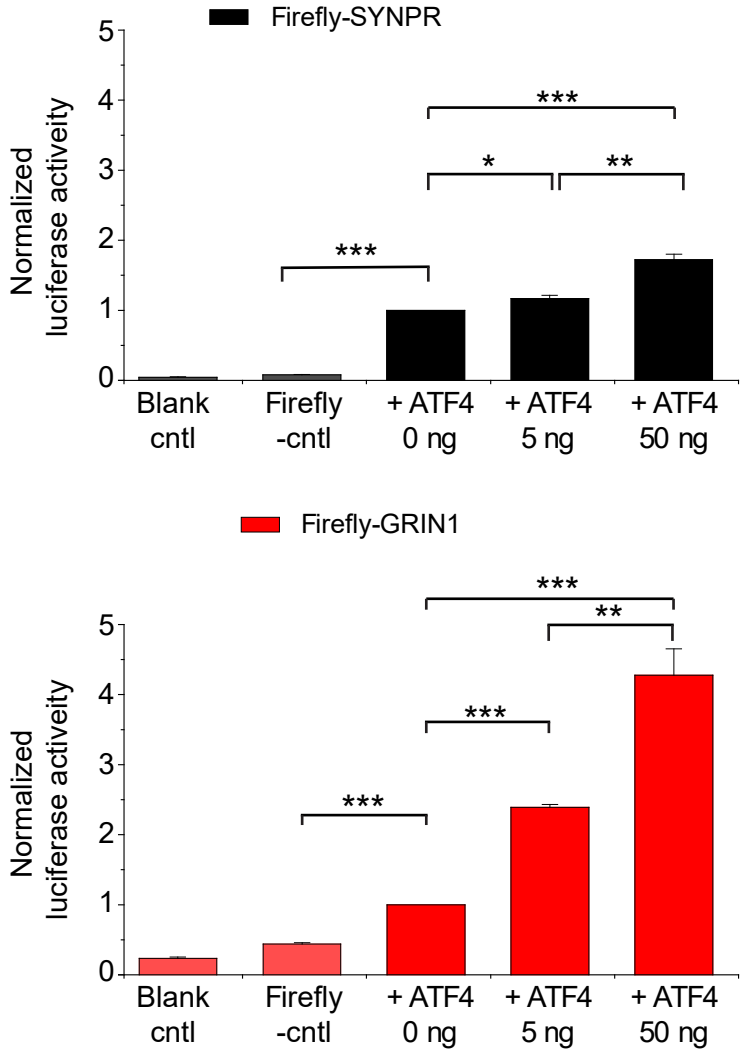

Supplementary Figure 4 (Wang et al.)

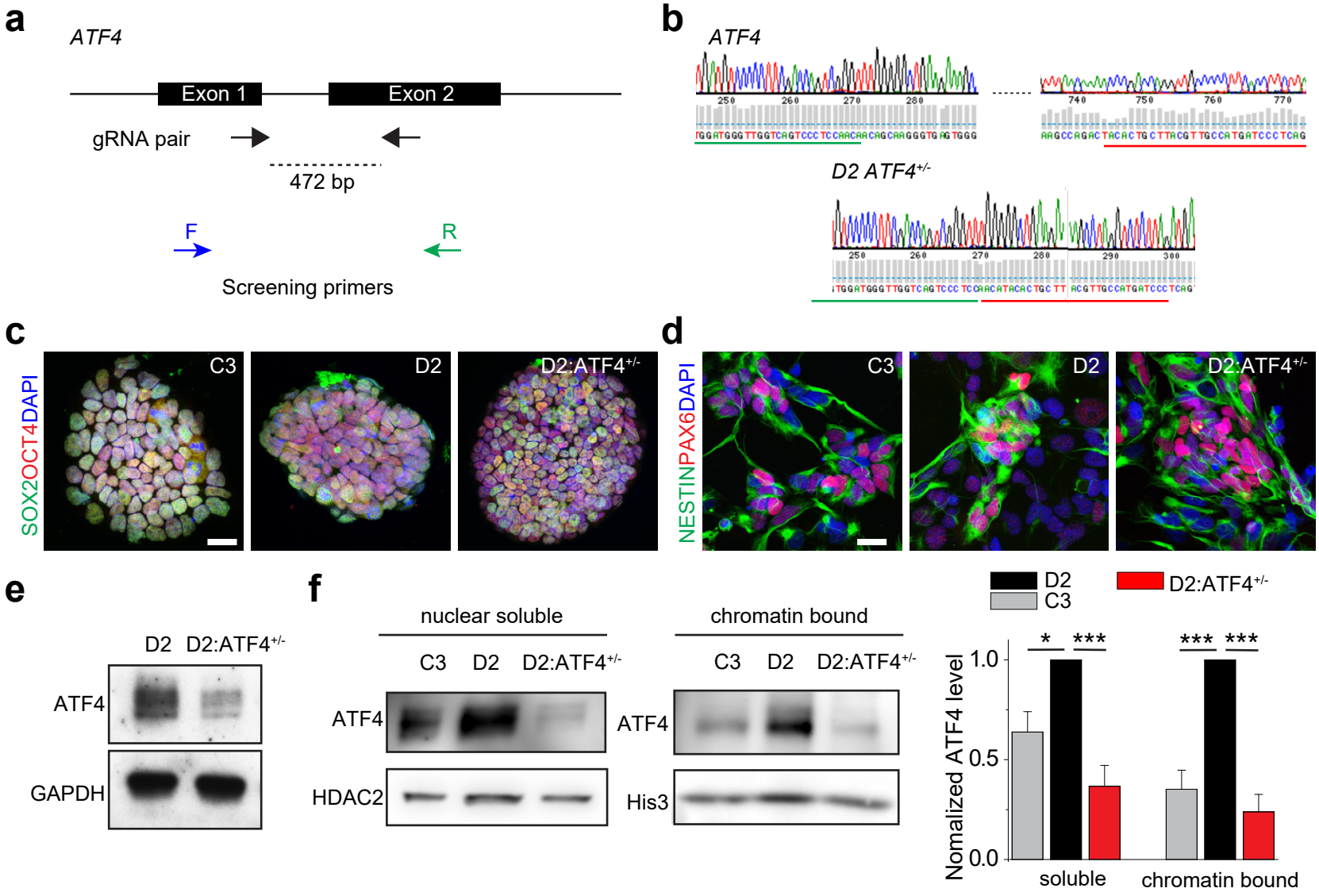

Supplementary Figure 5 (Wang et al.)

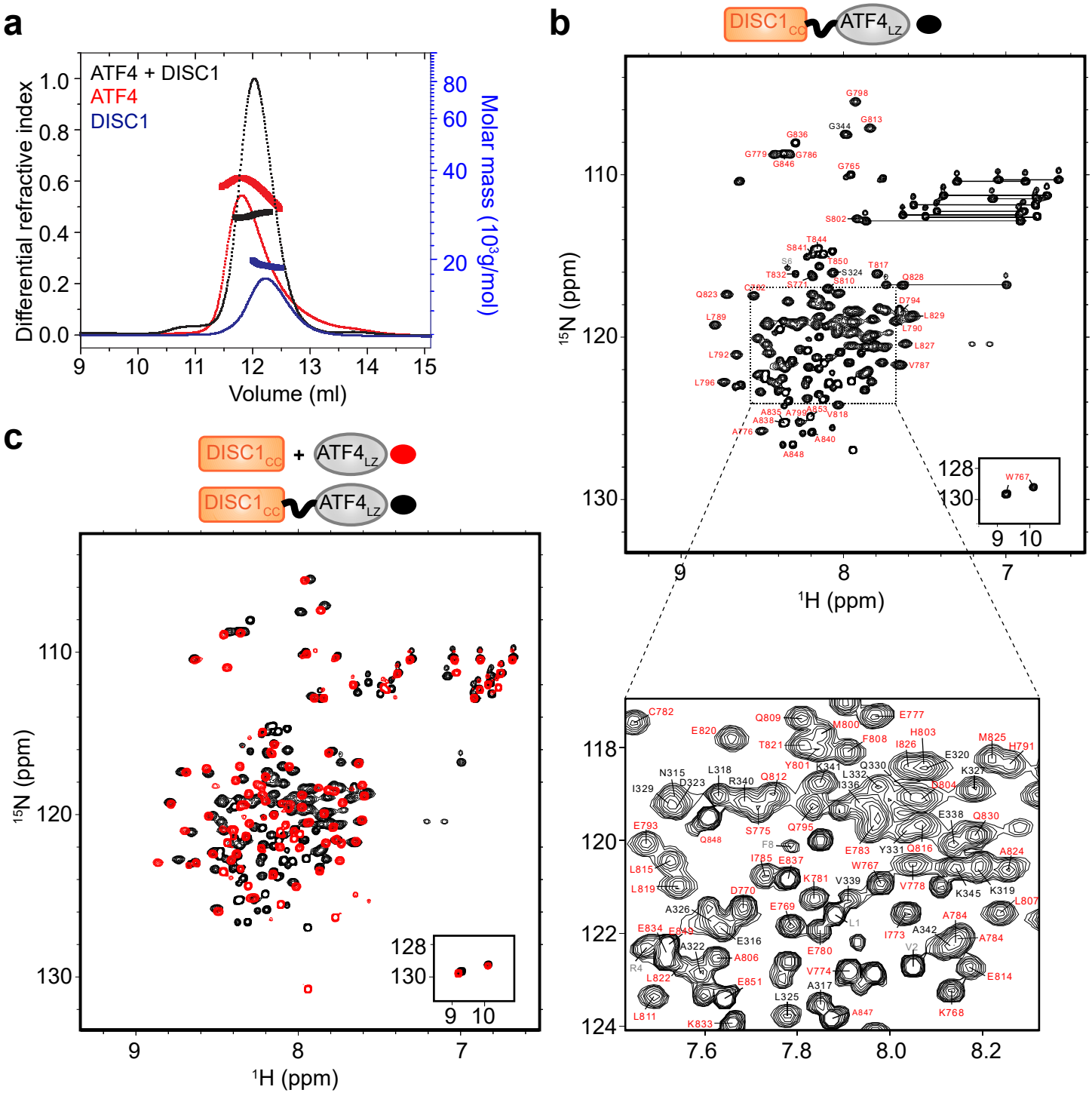

Supplementary Figure 6 (Wang et al.)

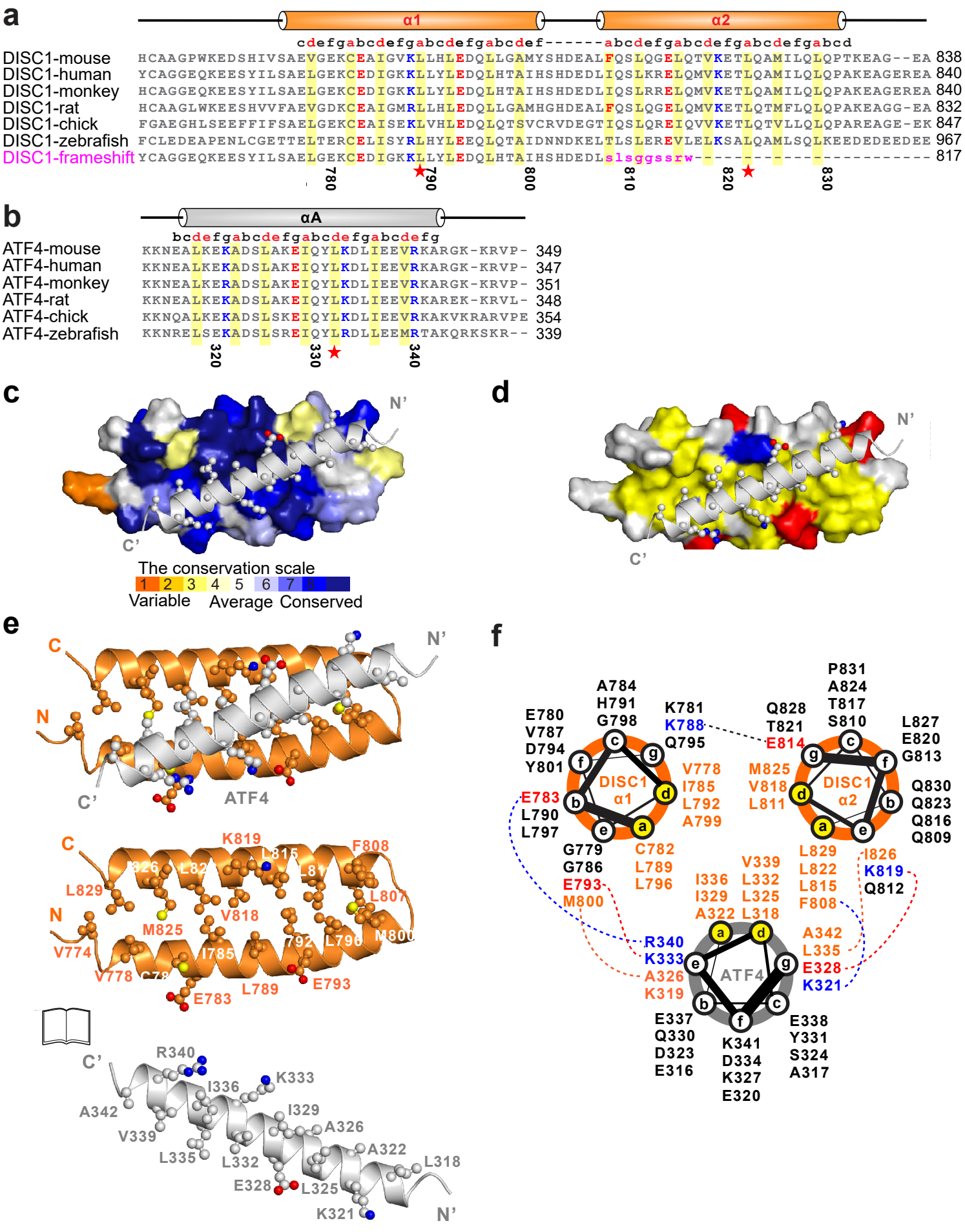

Supplementary Figure 7 (Wang et al.)

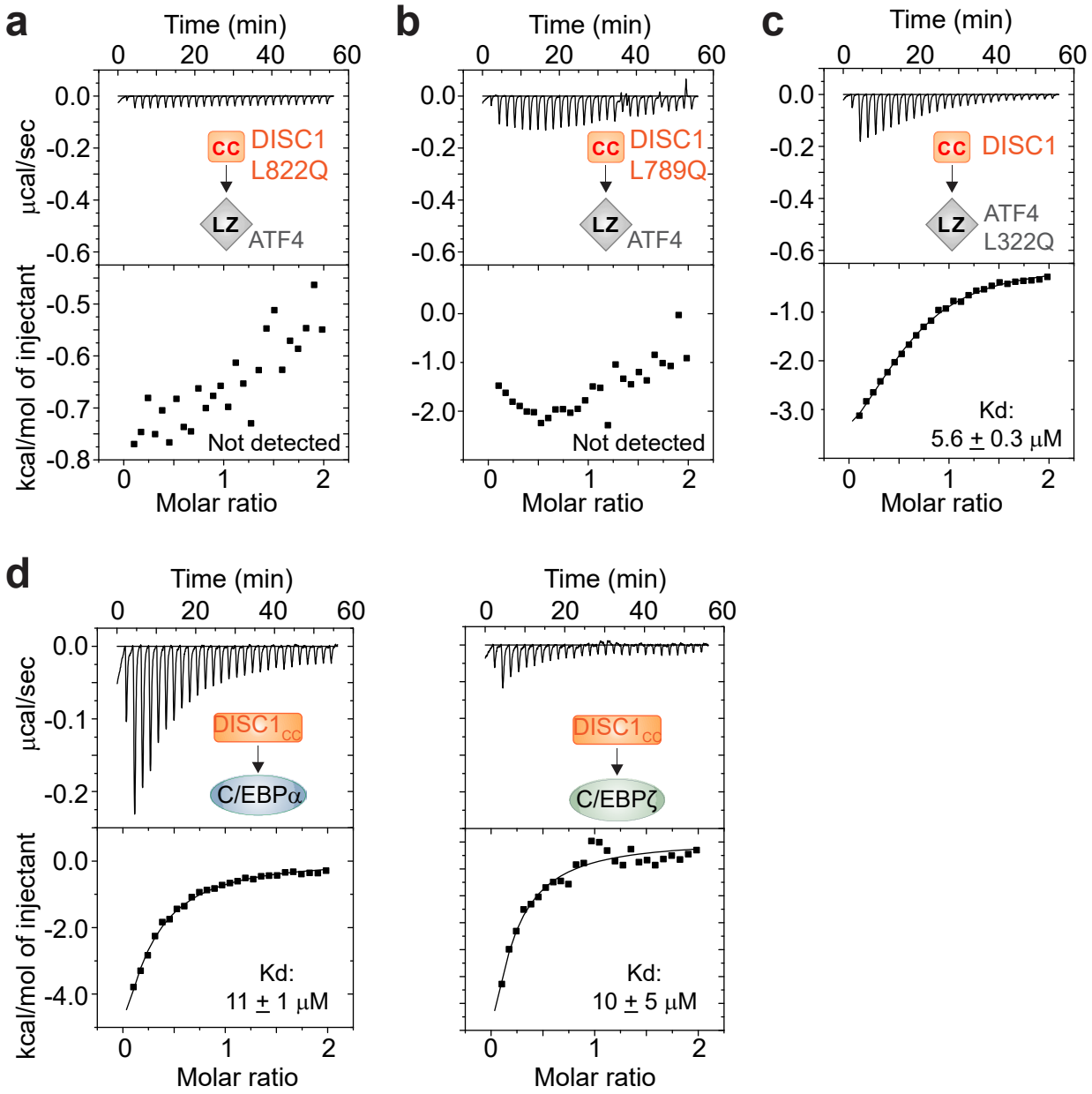

Supplementary Figure 8 (Wang et al.)